

# Propagation of $A_0$ Mode through the Front Edge of a Delamination: Numerical and Experimental Studies

Rakesh Kumar Singh<sup>1</sup> and Ramadas Chennamsetti<sup>2,#</sup>

<sup>1</sup> Faculty of Aeronautical Engineering (Mechanical), Air Force Technical College, Bangalore, India, 560-015

<sup>2</sup> Composites Research Center, R & D E (E), DRDO, Alandi Road, Dighi, Pune, India, 411-015

# Corresponding Author / E-mail: rd\_mech@yahoo.co.in, TEL: +91-20-2704-4875, FAX: +91-20-2704-4861

KEYWORDS: Lamb waves, Semi-infinite delamination, Power transmission coefficients, Transmission factors, Finite element analysis, Delamination edge

*Numerical and experimental studies carried out on the propagation of ultrasonic Lamb wave and its interaction with the front edge of a delamination in a cross-ply and unidirectional composite laminates are presented in this paper. When the fundamental anti-symmetric Lamb mode ( $A_0$ ) is incident at the leading (front) edge of a delamination, it undergoes reflection and transmission into the sub-laminates. Numerical simulations carried out on the interaction of the  $A_0$  mode with the edge of a semi-infinite delamination revealed that during this interaction,  $S_0$  mode is generated and propagate as  $A_0S_0$  (propagation of the  $S_0$  mode due to the incident  $A_0$  mode) mode in the top and bottom sub-laminates along with the incident  $A_0$  mode, which propagates as  $A_0A_0$  (propagation of the  $A_0$  mode due to the incident  $A_0$  mode) mode. Transmission factors and power transmission coefficients of  $A_0A_0$  and  $A_0S_0$  modes on an assortment of excitation frequencies – 150 kHz, 175 kHz, 200 kHz and 225 kHz, and thickness ratios were computed. Experimental validation of results arrived through numerical simulations, was also carried out employing air-coupled ultrasonic transducers.*

Manuscript received: November 12, 2013 / Revised: March 30, 2014 / Accepted: April 13, 2014

## 1. Introduction

One of the critical damages that laminated composites encounter is delamination. This damage is sub-surface in nature and difficult to identify with naked eye.<sup>1</sup> The presence of delamination in a structure debilitates the structure's performance. Detection of such a damage at an early stage helps in taking precautionary measures.

Lamb waves are ultrasonic waves which propagate through plate-like structures.<sup>2</sup> These waves have shown a promising picture for detection of delaminations.<sup>3-6</sup> Attempts have also been made to employ Lamb wave based scanning techniques to find out delaminations<sup>7-9</sup> in composite materials.

Lamb waves are dispersive; viz. velocity depends on the product of frequency and thickness. Depending on the relationship between the displacement profiles with thickness, Lamb modes are classified into symmetric ( $S_n$ ) and anti-symmetric ( $A_n$ ) modes. The specific order (represented by the subscript 'n') of these two mode types depend on the excitation frequency and thickness of a plate. Nonetheless, the multi-modal characteristics of Lamb waves pose some problems when they are used in Non-destructive Evaluation (NDE) applications. It was observed that when Lamb waves interact with defects, they undergo

mode conversion in addition to reduction in amplitude and change in arrival time.<sup>4,10-13</sup> Mode conversion, change in arrival time and amplitude completely depend on type of defect, geometry, orientation and kind of Lamb mode incident. Consequently, while employing a Lamb mode for flaw detection, it is necessary to appreciate the interaction between the Lamb mode and the flaw. This helps in identification of features of the Lamb mode that can be employed for locating and sizing of defects. When Lamb waves were employed for detection of delaminations, it was observed qualitatively that reflections take place at the rear edge of delamination. It was also found that mode conversion takes place at the front and rear edges of symmetric<sup>14</sup> and asymmetric delaminations<sup>15</sup> when  $A_0$  was incident at the delamination

From the above discussion it is surmised that no studies are available on the interaction of  $A_0$  mode with the front edge of a delamination and its transmission (amplitude and power) into the delamination region in a composite laminate. And also, it is not reported how the amplitude and power associated with the  $A_0$  mode, which is propagating from the front edge to the rear edge of the delamination, vary with the location of the delamination across the laminate thickness, as well as in relation with the excitation frequency. Therefore, the present work focuses on the interaction and transmission (both amplitude and power) of the  $A_0$

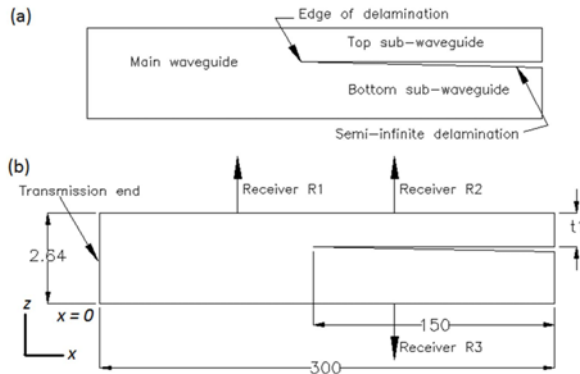


Fig. 1 (a) Semi-infinite delamination with its edge, (b) Model used for numerical simulations

mode when incident at the front edge of the delamination in a composite laminate. Detailed studies were carried out to understand the transmission characteristics of the  $A_0$  mode when transmitted from main laminate to sub-laminates at various excitation frequencies. During the interaction of the  $A_0$  mode with the front edge of a delamination,  $S_0$  mode (mode converted  $A_0$  mode) was also generated. The  $S_0$  mode propagates in the sub-laminates along with the incident  $A_0$  mode. Studies were performed to understand the transmission behaviour of the  $S_0$  mode in the sub-laminates at various excitation frequencies.

## 2. Simulation of Lamb Mode Propagation

In general, a delamination in a structure has both the edges (front and rear). At the delamination location, the laminate (main waveguide) is divided into two sub-laminates (sub-waveguides). The wave incident at the front edge of the delamination propagates through the sub-waveguides and undergoes reflection and transmission at the rear edge of the delamination.<sup>10,12,14,15</sup> If the length of the delamination is short, the forward travelling wave groups undergo interference with those reflected at the rear edge of the delamination. It is difficult to separate the wave groups, which underwent interference. Hence, to circumvent this, the size of delamination selected was half of the length of the specimen. The delamination starts from one of the ends of the specimen up to the middle of the specimen as shown in Fig. 1(a). Since the length of the selected delamination was large and it had one edge only, it was termed as 'semi-infinite delamination'.<sup>11</sup> Consequently, the wave groups propagating through the front edge of delamination do not undergo interference with those reflected from the edge of the specimen.

### 2.1 Finite element model

Two dimensional numerical simulations of Lamb wave propagation through the front edge of a delamination in unidirectional (UD) and cross-ply laminates were carried out using the Finite Element (FE) code, ANSYS. The details of the model are as follows. Material of the model was glass fibres and epoxy resin, whose lamina level properties<sup>9</sup> are given in Table 1. The thickness of each ply was 0.33 mm. In UD laminate, eight unidirectional plies were stacked to get a 2.64 mm thick laminate thickness. The stacking sequence in cross-ply laminate was  $[0/90/0/90]_s$ . Since there were eight plies in the cross-ply laminate, the

Table 1 Material properties<sup>9</sup>

$E_{11}$ GPa	$E_{22}$ GPa	$\nu_{12}$	$\nu_{23}$	$G_{12}$ GPa	$\rho$ kg/m <sup>3</sup>
44.68	6.90	0.280	0.355	2.54	1990

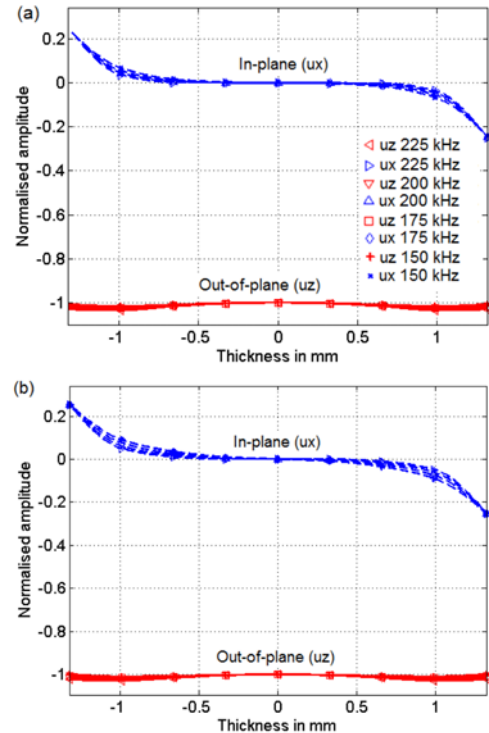


Fig. 2 Displacement profile across thickness of (a) UD and (b) cross-ply laminates to excite  $A_0$  mode

total thickness of the laminate worked out to be 2.64 mm. The length of the model and the size of semi-infinite delamination were 300 mm and 150 mm, respectively as shown in Fig. 1(b). In the model, each ply was modelled and its properties were assigned. Since each laminate contains a total number of eight plies, it is possible to have the delamination at any one of the interfaces across the thickness. The delamination has been modelled by de-merging the nodes at that location. Since the semi-infinite delamination divides the main laminate into sub-laminates, the stacking sequence of plies and the thickness of each sub-laminate depend on the location of the interface of delamination.

The element used for meshing was a four node plane strain element. It has two translatory Degree-of-Freedom (DoF) - one in  $x$  direction and the other on in  $z$  direction as shown in Fig. 1(b). Albeit ANSYS is an implicit code, element mesh size and time step size were calculated using Blake's and CFL (Courant, Federich and Lewis) criteria. The size of the elements was 0.165 mm in the thickness direction and 0.25 mm in the length direction. The time step was 50 nano sec. Time marching was carried out using Newmark's time integration technique. Attenuation or damping was not considered in numerical modelling.

### 2.2 Excitation details

The mode of excitation was  $A_0$  Lamb mode, and the range of frequency of excitation was 150 kHz to 225 kHz in steps of 25 kHz. There were five cycles in the excitation pulse. Therefore, the durations

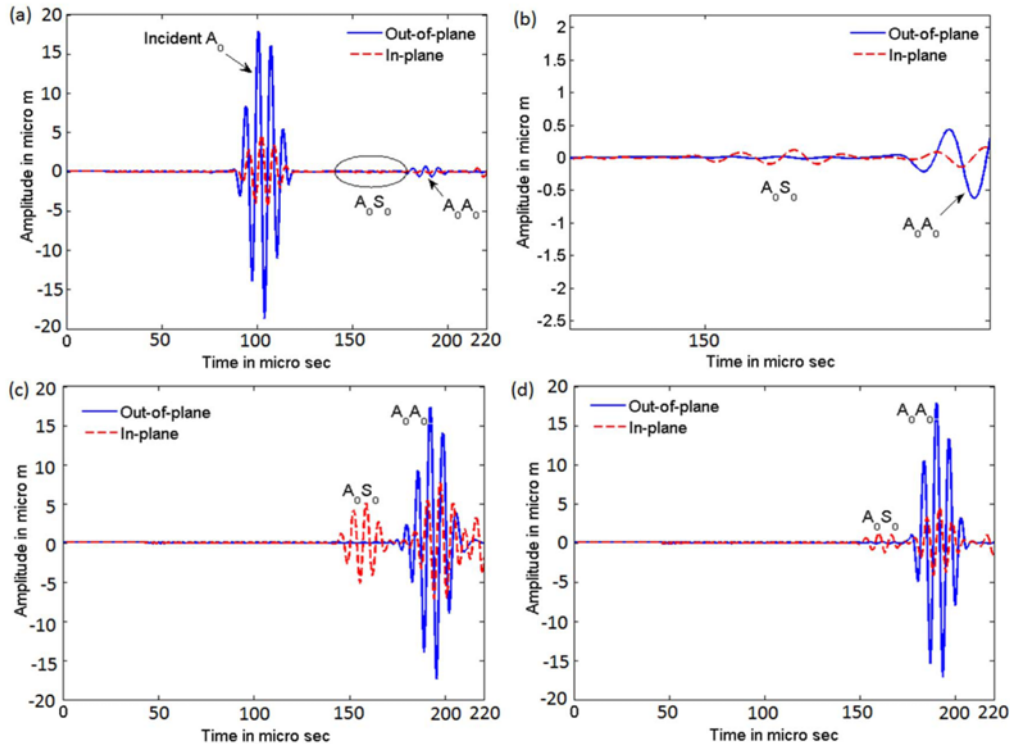


Fig. 3 A-scans captured at (a) R1, (c) R2 and (d) R3. (b) Shows zoomed portion of A-scan at R1

of excitation were  $33.33 \mu\text{s}$ ,  $28.57 \mu\text{s}$ ,  $25 \mu\text{s}$  and  $22.22 \mu\text{s}$  for the excitation frequencies of 150 kHz, 175 kHz, 200 kHz and 225 kHz, respectively. The excitation frequencies were so chosen, to ensure that only the fundamental modes ( $A_0$  and  $S_0$ ) exist. The excitation pulse was a tone burst modulated with a Hanning window. In the FE analysis, the  $A_0$  mode was excited at  $x=0$ , as shown in Fig. 1(b), by giving displacement profile across the thickness, as shown in Fig. 2. Three receivers, R1, R2 and R3 were deployed at  $x=100 \text{ mm}$  and  $x=200 \text{ mm}$  as shown in Fig. 1(b). The in-plane ( $u_x$ ) and out-of-plane ( $u_z$ ) displacement time histories were captured at all the receivers.

### 2.3 Wave interaction with the edge

Initially, in order to validate the FE model, a set of numerical simulations were carried out on a defect free cross-ply and UD laminates and also on all different sub-laminates to estimate the group velocities of  $A_0$  and  $S_0$  modes at various excitation frequencies. The group velocities thus obtained were in close agreement with those from DISPERSE.<sup>16</sup> The following paragraph delineates the numerical simulations carried out with 150 kHz as excitation frequency on the cross-ply laminate having a semi-infinite delamination between the plies [0] (first) and [90] (second) from the top surface. Due to the presence of the semi-infinite delamination, the stacking sequence of the plies in the top and bottom sub-laminates was [0] and [90/0/90/90/0/90/0], respectively. The group velocities of ( $A_0$ ,  $S_0$ ) modes in the sub-laminates [0] and [90/0/90/90/0/90/0], computed through numerical simulations, were (1149 m/s, 5090 m/s) and (1124 m/s, 2917 m/s), respectively.

$A_0$  mode was excited at  $x=0$  (transmission end) by giving appropriate displacement profile as shown in Fig. 2. When the  $A_0$  propagating in the main laminate (healthy region) interacts with the edge of a delamination, it gets reflected back into the main laminate and also

transmits into the top and bottom sub-laminates at the edge of the semi-infinite delamination. At the same time, the incident mode undergoes mode conversion to  $S_0$  mode, which also reflects back into the main laminate and transmits into the top and bottom sub-laminates along with the incident  $A_0$  mode. Since the genesis of  $S_0$  mode at the edge was due to the incident  $A_0$  mode, the propagating  $S_0$  mode was named as  $A_0S_0$  mode.<sup>14</sup> Similarly, the propagation of the reflected  $A_0$  mode in the main laminate and propagation of the transmitted  $A_0$  mode in the top and bottom sub-laminates was because of the incident  $A_0$  mode. Therefore, these  $A_0$  modes were named  $A_0A_0$  modes.<sup>14</sup>

### 2.4 A-scans from numerical simulations

At receivers R1, R2 and R3, both the in-plane and out-of-plane displacement component time histories (A-scan), shown in Fig. 3, were captured. There are two wave groups, the incident  $A_0$  mode and reflected  $A_0A_0$  mode, in the A-scan, captured at R1, as shown in Fig. 3(a). When a portion of the A-scan is zoomed just before the appearance of  $A_0A_0$  mode, as shown in Fig. 3(a), the  $A_0S_0$  mode (mode converted  $A_0$ ) was detected, as shown in Fig. 3(b). Since amplitude of  $A_0S_0$  mode is one tenth of the  $A_0A_0$  mode, it is difficult to identify the former in the A-scan in Fig. 3(a). Moreover, amplitude of  $A_0A_0$  mode itself is nearly  $1/20^{\text{th}}$  of the incident  $A_0$  mode. To confirm the propagation of  $A_0A_0$  and  $A_0S_0$  modes in the main laminate, their arrival times at R1 from the A-scan ( $188.7 \mu\text{s}$ ,  $161.5 \mu\text{s}$ ) were compared with that computed using group velocities ( $185.06 \mu\text{s}$ ,  $156.5 \mu\text{s}$ ), and they were found to be in a close match with each other.

Fig. 3(c) shows A-scan captured at receiver R2 positioned over the top sub-laminate. The first and the second wave groups in the A-scan are transmitted  $A_0S_0$  and  $A_0A_0$  modes, respectively. To validate this, arrival times of the wave groups from the A-scan ( $156.89 \mu\text{s}$ ,  $193.65$

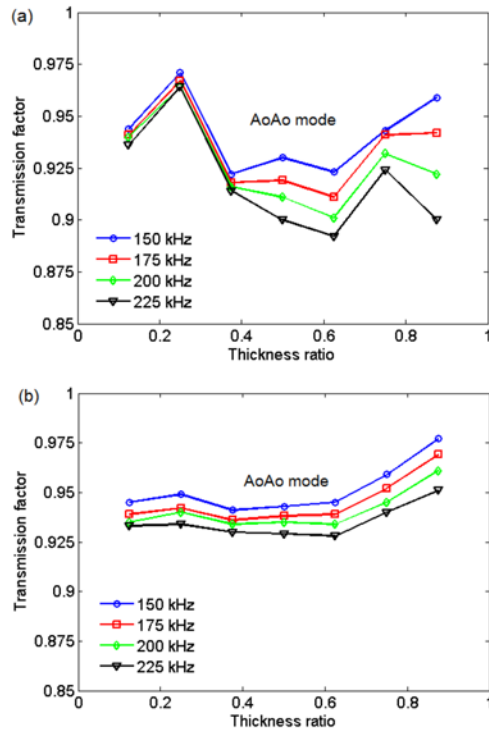


Fig. 4 Variation in transmission factor of  $A_0A_0$  mode in (a) cross-ply and (b) UD laminates

$\mu\text{s}$ ) were compared with that computed using group velocities (158.12  $\mu\text{s}$ , 194.90  $\mu\text{s}$ ) and found to be in accord with each other.

Two wave groups,  $A_0S_0$  and  $A_0A_0$  shown in A-scan (Fig. 3(d)), which was recorded at receiver R3, were found to be propagating in the bottom sub-laminate. To prove this, arrival times of the wave groups from the A-scan (161.12  $\mu\text{s}$ , 190.85  $\mu\text{s}$ ) were compared with those estimated using group velocities (162.35  $\mu\text{s}$ , 192.09  $\mu\text{s}$ ), and were found to be in concurrence.

In each laminate there were eight plies. Therefore, the semi-infinite delamination can be anywhere between any two consecutive plies. Therefore, numerical simulations akin to the above were performed introducing the delamination between each interface of the plies in the cross-ply and UD laminates at four excitation frequencies (150 kHz, 175 kHz, 200 kHz and 225 kHz). In each numerical simulation, the incident  $A_0$  mode underwent mode conversion to  $S_0$  mode and  $A_0A_0$  and  $A_0S_0$  wave groups were propagating in the main, the top and the bottom sub-laminates. In each simulation case, the arrival times of  $A_0A_0$  and  $A_0S_0$  modes from A-scans were compared with that computed analytically, and it was found that they were in concurrence with each other.

### 3. Analysis of Numerical Simulated Data

#### 3.1 Transmission factors

In each numerical simulation, A-scans were captured over the main laminate and the sub-laminates. Amplitude of  $A_0$  wave group in each A-scan was computed in the frequency domain by performing Fourier Transform (FT) on the wave group. Transmission factor of  $A_0A_0$  mode

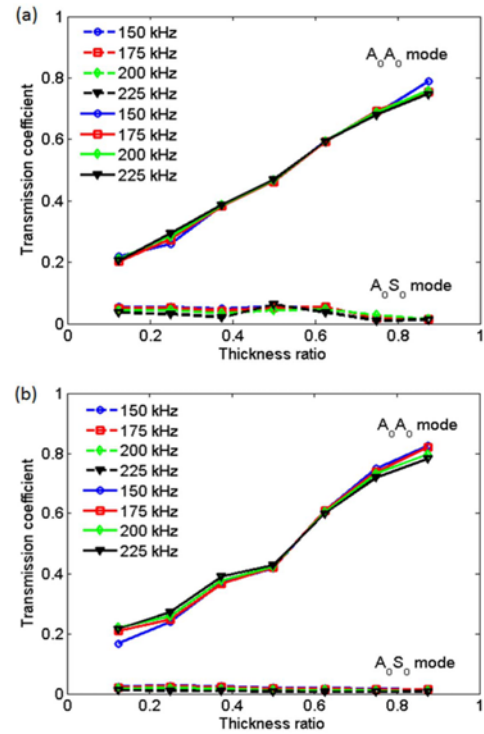


Fig. 5 Variation in power transmission coefficient of  $A_0A_0$  and  $A_0S_0$  modes in (a) cross-ply and (b) UD laminates

propagating in the sub-laminates is defined as the ratio between the amplitude of the  $A_0A_0$  mode and the incident  $A_0$  mode. Fig. 4 shows variation in transmission factor of  $A_0A_0$  mode with thickness ratio, which is defined as the ratio of the thickness of the sub-laminate over which the receiver was placed (A-scan captured) to the thickness of the main laminate.

#### 3.2 Transmission Coefficients

Moreover, the power associated with the incident  $A_0$  mode was estimated in all the numerical simulations. At the edge of the semi-infinite delamination, the incident power is distributed among  $A_0A_0$  and  $A_0S_0$  modes propagating in the top and the bottom sub-laminates, and also the wave groups reflected back into the main laminate. However, the power associated with the reflected wave groups is very less compared to that associated with the wave groups  $A_0A_0$  and  $A_0S_0$  propagating in the sub-laminates. Hence, the power associated with the wave groups propagating in the sub-laminates only was considered. Power transmission coefficient is defined as the ratio of the power associated with the transmitted wave group to that associated with the incident wave group. Fig. 5 shows variation in power transmission coefficient with the thickness ratio.

### 4. Experimental Work

#### 4.1 Preparation of specimens

Experiments were carried out on Glass Fibre Reinforce Plastic (GFRP) cross-ply and UD laminates having ply stacking as  $[0/90/0/90]_s$  and  $[0_4]_s$ , respectively. The thickness of each lamina (ply) was 0.33 mm.

Since there were eight plies in each laminate, the total thickness of each laminate was 2.64 mm. Lamina level properties of GFRP material are listed in Table 1. Four laminates - two cross ply and two UD were fabricated using Resin Film Infusion (RFI) technique. In the first cross-ply laminate, semi-infinite delamination was introduced between the first and the second plies, whereas in the second cross-ply laminate it was in between the third and the fourth plies. The delaminations in the cross-ply laminates result in the thickness ratios (0.125, 0.875) and (0.375, 0.625) in the first and second laminates, respectively. In case of UD laminates, the delaminations were in between the second and the third plies in the first UD laminate and in between the fourth and the fifth plies in the second UD laminate. The thickness ratios corresponding to the delaminations introduced in the UD laminates were (0.250, 0.750) and (0.500, 0.500) in the first and the second laminates, respectively.

In the following paragraph, the process followed to fabricate the first cross-ply laminate with the semi-infinite delamination using RFI process, is detailed.

A resin film was sandwiched between two plies, which were oriented in the desired directions. Such sandwiches were placed one above the other till the desired thickness was attained. A brass strip of 0.05 mm thick, 180 mm length and 130 mm width was inserted between [0] and [90] degree plies from one of the sides of the laminate in such a way that 150 mm and 100 mm were inside and 30 mm on each side was projecting out. The brass strip was coated with PVA (Poly Vinyl Alcohol) for easy removal from the laminate after curing. Sufficient bleeder was used to absorb any excess resin. A vacuum bag was placed on the top and sealed with a sealant tape. A thermocouple was placed on the top of the sample to continuously monitor the temperature during curing. The sample was heated at a rate of 2°C/min up to 80°C, soaked for 30 minutes followed by re-heating up to 120°C and finally soaked for 60 minutes. After completion of heating cycle, the sample was allowed to cool to room temperature. The brass strip was carefully removed by subjecting to four point bending. Thus a delamination of approximate size 150×100 mm<sup>2</sup> was created in the laminate. The final dimensions of the laminate obtained after cutting were 300×200 mm<sup>2</sup>. Fig. 5(a) shows the laminates realised using the above discussed process.

#### 4.2 Experimental setup

The experimental set up consists of a signal generator, power amplifier, 100 MHz A/D card, signal conditioner and a desk top computer. The probes used were air-coupled ultrasonic transducers with a central frequency of 200 kHz, provided by Ultrason Group, USA. Probe holding fixture was fabricated using perspex sheet to hold the air-coupled ultrasonic probes. This was a probe unit. The angle of the transducer to be set to transmit and receive  $A_0$  was calculated using Snell's law. The probes were arranged to receive  $A_0$  wave group in pitch-catch arrangement as shown in Fig. 6(b).

#### 4.3 Measurement of $A_0$ mode velocity

At first, to check the transmission and reception of  $A_0$  mode in the laminates, the group velocity of  $A_0$  mode in the cross-ply laminate was determined experimentally. The distance of separation between the transmitter and the receiver was fixed at 80 mm. At this distance,  $A_0$  mode took 98.6 ms to reach the receiver. Afterwards, the distance of

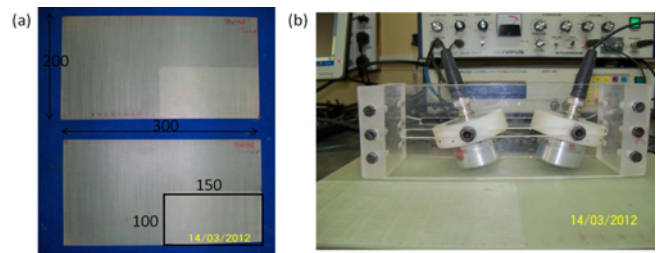


Fig. 6 (a) Specimens prepared using RFI process, (b) air-coupled probes fixed and oriented in a probe holder to capture  $A_0$  mode

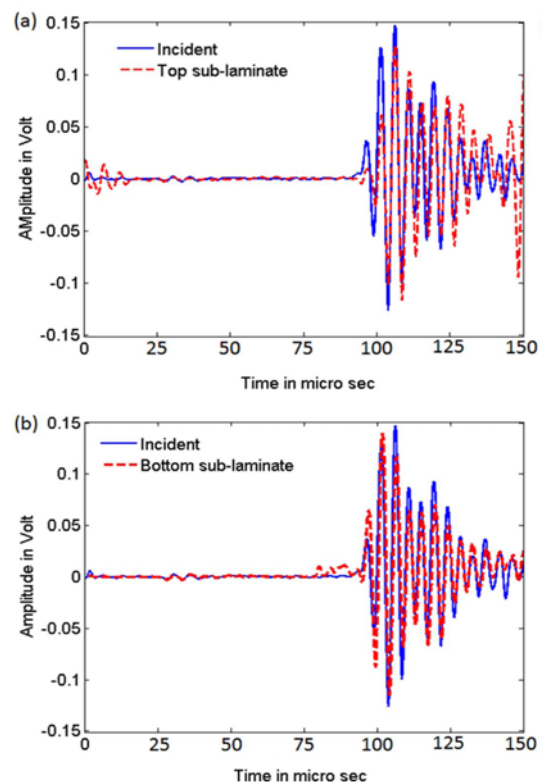


Fig. 7 A-scans obtained from experiments showing  $A_0$  mode captured over (a) the top sub-laminate and (b) the bottom sub-laminate

separation was changed to 120 mm. In this configuration the  $A_0$  mode reached the receiver at 134.5 ms. From these measurements, the group velocity of  $A_0$  mode was estimated to be 1114.2 m/s, which is in accord with the group velocity of  $A_0$  mode from numerical simulations (1156 m/s) and DISPERSE (1138 m/s).

#### 4.4 A-Scans from experiments

Following depicts the experimental A-scans captured over the second cross-ply laminate, which had semi-infinite delamination between the third and the fourth plies. The probes were oriented to generate and receive  $A_0$  mode. Initially, both the transmitter and receiver were positioned over the main laminate. This was the incident mode at the edge of the semi-infinite delamination as shown in Fig. 7. Amplitude of this mode was taken as the reference value.

Now, the probe unit was moved in such a manner that the transmitter was on the main laminate and the receiver over the top sub-laminate,

whose lay-up was  $[0/90/0]$ . The receiver over the top sub-laminate was reoriented to receive  $A_0$  mode. One A-scan recorded in this configuration is shown in Fig. 7(a). The wave group in this A-scan is  $A_0A_0$  mode. Later, the laminate was turned upside down. Again, the transmitter and the receiver were positioned in such a manner that the transmitter and the receiver were over the main laminate and the sub-laminate (lay-up  $[90/90/0/90/0]$ ), respectively. Fig. 7(b) shows wave group,  $A_0A_0$  mode, captured in this configuration.

Experimental procedure depicted above was followed to capture A-scans in the remaining three laminates (one cross-ply laminate and two UD laminates). In each laminate amplitude of  $A_0$  mode, which was captured over the healthy region (main laminate), was taken as the reference value to compute transmission factor in the frequency domain.

## 5. Results and Discussion

From numerical simulations carried out on cross-ply and UD laminates with various locations of interface delamination across the thickness of the laminates, it was observed that during the interaction of  $A_0$  mode, which propagates in the main laminate, with the edge of a semi-infinite delamination, it undergoes mode conversion to  $S_0$  mode. Besides, the incident  $A_0$  mode reflects back into the main laminate and also transmits into the sub-laminates along with the generated (converted)  $S_0$  mode. The reflected and transmitted modes in the main laminate and the sub-laminates, respectively, propagate as  $A_0A_0$  and  $A_0S_0$  modes. Furthermore, to verify the propagation of these modes in the main and the sub-laminates, arrival times from A-scans were compared with those computed using group velocities, and found to be in close agreement with each other.

It was also noticed that amplitudes of the reflected  $A_0A_0$  and  $A_0S_0$  modes propagating in the main laminate are negligibly small compared to the amplitudes of all other wave groups. However, the amplitudes (expressed in terms of transmission factors in frequency domain) of  $A_0A_0$  modes, which are propagating in various sub-laminates of both UD and cross-ply laminates, are nearly in the range of 90% of the amplitude of the incident  $A_0$  mode as shown in Fig. 4. It is also clear from Fig. 4 that the transmission factors are nearly independent of the thickness ratio and frequency.

To examine further the propagation of characteristics of  $A_0A_0$  and  $A_0S_0$  modes in the sub-laminates, the power associated with each wave group was computed and expressed in terms of power transmission coefficient. Fig. 5 shows variation in power transmission coefficients of  $A_0S_0$  and  $A_0A_0$  modes with the thickness ratio in cross-ply and UD laminates. It is noticed that variation in power transmission coefficient of  $A_0S_0$  mode with the thickness ratio and frequency is negligible. And also, the power associated with  $A_0S_0$  modes in both cross-ply and UD was less than 2% of the incident power. However, the power carried by  $A_0A_0$  mode significantly depends on the thickness ratio, but nearly independent of the excitation frequency as shown in Fig. 5. When the thickness ratio is 0.125, the power associated with  $A_0A_0$  mode is approximately 20% of the incident power. At 0.875 thickness ratio,  $A_0A_0$  mode carries nearly 80% of the incident power.

To verify the observations made in numerical simulations,

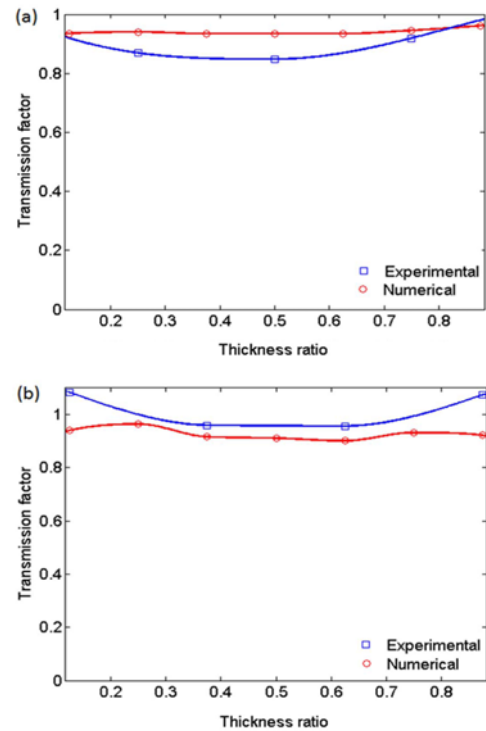


Fig. 8 Variation in transmission factors of  $A_0A_0$  mode from numerical simulations and experiments in (a) UD and (c) cross-ply laminates

experiments were performed on cross-ply and UD laminate employing air-coupled transducers. Four laminates (two UD and two cross-ply) with semi-finite delaminations were realised using RFI process. The locations of the semi-infinite delamination in the four laminates resulted in three and four thickness ratios in UD and cross-ply laminates, respectively. A-scans were captured orienting the probe unit in various configurations. The transmission factors of experimentally captured  $A_0A_0$  mode were estimated and their variation with the thickness ratio is plotted along with the numerically simulated transmission factors as shown in Fig. 8.

It is clear that the amplitude of the transmitted  $A_0A_0$  mode in UD laminate was nearly 85–90% of the amplitude of the incident mode, whereas from numerical simulations it was found to be approximately 90–95%. In cross-ply laminate the transmission factor was slightly higher than that in UD laminate. Moreover, the transmission factors in cross-ply laminate from experiments and numerical simulations are nearly 0.93 and 0.98, respectively. A small mismatch in numerical simulations and experiments was attributed to attenuation of the Lamb modes, which was not considered in numerical modelling. Moreover, there was a little warping in the sub-laminates (experimental specimens), since their lay-ups were not symmetric. Experiments were repeated several times to check the reproducibility and repeatability. It was found that experimental results were both repeatable and reproducible.

From numerical simulations followed by experimental results, it is inferred that higher power transmission takes place through the thicker (higher thickness ratio) sub-waveguide compared to the thinner (lower thickness ratio) sub-waveguide. A possible reason for this is the difference in phase velocity of  $A_0$  mode in the main waveguide and the thick sub-waveguide is less as compared to that, in the main and the

thin sub-waveguide. And also, the cross-sectional area of the thicker wave guide is more than the thinner one. However, the transmission factor is independent of the thickness of the sub-waveguide and difference in phase velocity of  $A_0$  mode in the main waveguide and the sub-waveguide.

## 6. Conclusions

It is concluded that when  $A_0$  mode is incident at the front edge of a delamination, it undergoes mode conversion, reflection into the main waveguide and transmission into the sub-waveguides along with the mode converted mode. Amplitude of the reflected modes from the front edge is very low. Amplitude of the transmitted  $A_0$  modes into the sub-wave guides is 90–95% of the incident  $A_0$  mode amplitude. Moreover, the amplitude of the  $A_0$  mode in the sub-waveguide is nearly independent of the thickness ratio, excitation frequency and also stacking sequence. In case of power transmission, more power is carried by the transmitted  $A_0$  mode through thicker waveguide. Furthermore, power carried by the mode converted  $A_0$  mode ( $S_0$  mode) propagating in the sub-waveguides is less than 2% of the incident power at the edge of the delamination. Besides, the power carried by the  $S_0$  mode in the sub-waveguides is nearly independent of the excitation frequency.

Since the amplitude of the reflected modes from the front edge of a delamination is negligible, if  $A_0$  mode is employed for detection of delaminations in a composite laminate, it is difficult to identify the reflected modes from the front edge of the delamination. Besides, the transmitted modes in the sub-waveguides propagate as if they have not encountered any delamination in their path of propagation.

## ACKNOWLEDGEMENT

Authors acknowledge Mr. Vinod Durai Swamy, from R&DE(E), for making the laminates. The authors thank Mr. Avinash Hood and Mr. Irfan Khan, both from R&DE(E), for their help in experimental work.

## REFERENCES

- Sridharan, S., "Delamination Behaviour of Composites," Elsevier, 2008.
- Nayfeh, A. H., "Wave Propagation in Layered Anisotropic Media: With Application to Composites," Elsevier, 1995.
- Raišutis, R., Kažys, R., Žukauskas, E., and Mažeika, L., "Ultrasonic Air-Coupled Testing of Square-Shape CFRP Composite Rods by Means of Guided Waves," *Ndt & E International*, Vol. 44, No. 7, pp. 645-654, 2011.
- Hu, N., Shimomukai, T., Yan, C., and Fukunaga, H., "Identification of Delamination Position in Cross-Ply Laminated Composite Beams using  $S_0$  Lamb Mode," *Composites Science and Technology*, Vol. 68, No. 6, pp. 1548-1554, 2008.
- Kundu, T., Ehsani, M., Maslov, K., and Guo, D., "C-Scan and L-Scan Generated Images of the Concrete/GFRP Composite Interface," *NDT & E International*, Vol. 32, No. 2, pp. 61-69, 1999.
- Su, Z. and Ye, L., "Lamb Wave-based Quantitative Identification of Delamination in CF/EP Composite Structures using Artificial Neural Algorithm," *Composite Structures*, Vol. 66, No. 1, pp. 627-637, 2004.
- Castaings, M., Cawley, P., Farlow, R., and Hayward, G., "Single Sided Inspection of Composite Materials using Air Coupled Ultrasound," *Journal of Nondestructive Evaluation*, Vol. 17, No. 1, pp. 37-45, 1998.
- Toyama, N. and Takatsubo, J., "Lamb Wave Method for Quick Inspection of Impact-Induced Delamination in Composite Laminates," *Composites Science and Technology*, Vol. 64, No. 9, pp. 1293-1300, 2004.
- Ramadas, C., Padiyar, J., Balasubramaniam, K., Joshi, M., and Krishnamurthy, C., "Lamb Wave based Ultrasonic Imaging of Interface Delamination in a Composite T-Joint," *NDT & E International*, Vol. 44, No. 6, pp. 523-530, 2011.
- Hayashi, T. and Kawashima, K., "Multiple Reflections of Lamb Waves at a Delamination," *Ultrasonics*, Vol. 40, No. 1, pp. 193-197, 2002.
- Yuan, W. C., Zhou, L., and Yuan, F. G., "Wave Reflection and Transmission in Composite Beams Containing Semi-Infinite Delamination," *Journal of Sound and Vibration*, Vol. 313, No. 3, pp. 676-695, 2008.
- Ip, K. H. and Mai, Y. W., "Delamination Detection in Smart Composite Beams using Lamb Waves," *Smart Materials and Structures*, Vol. 13, No. 3, pp. 544, 2004.
- Castaings, M., Singh, D., and Viot, P., "Sizing of Impact Damages in Composite Materials using Ultrasonic Guided Waves," *NDT & E International*, Vol. 46, pp. 22-31, 2012.
- Ramadas, C., Balasubramaniam, K., Joshi, M., and Krishnamurthy, C., "Interaction of the Primary Anti-Symmetric Lamb Mode ( $A_0$ ) with Symmetric Delaminations: Numerical and Experimental Studies," *Smart Materials and Structures*, Vol. 18, No. 8, Paper No. 085011, 2009.
- Ramadas, C., Balasubramaniam, K., Joshi, M., and Krishnamurthy, C., "Interaction of Guided Lamb Waves with an Asymmetrically Located Delamination in a Laminated Composite Plate," *Smart Materials and Structures*, Vol. 19, No. 6, Paper No. 065009, 2010.
- Lowe, M., "Disperse Software," Imperial College London, 2003.